nanomaterials

MDPI

Article

Impact of Carbon Diffusion Induced Stress on the Properties of Diamond/GaN Heterojunctions

Haolun Sun [1], Mei Wu [1,*], Peng Xu [2], Chao Yuan [2], Ling Yang [1], Hao Lu [1], Bin Hou [1], Meng Zhang [1], Xiaohua Ma [1] and Yue Hao [1]

[1] National Engineering Research Center of Wide Band-Gap Semiconductor, Faculty of Integrated Circuit, Xidian University, Xi'an 710126, China; haolun_sun@stu.xidian.edu.cn (H.S.)
[2] School of Integrated Circuits, Wuhan University, Wuhan 430072, China
* Correspondence: wumei@xidian.edu.cn

Abstract

Integrating diamond with GaN provides an effective pathway to mitigate self-heating. However, the thermal boundary resistance (TBR) remains a persistent bottleneck for further heat dissipation. While carbon (C) diffusion into the SiNx interlayer is known to reduce TBR, the associated stress evolution and its impact on device performance remain underexplored. In this work, the synergistic regulation of heat transport and electrical performance induced by C diffusion was systematically investigated. Transmission electron microscopy (TEM) was employed to characterize the interfacial microstructure and the influence of C diffusion on the interface. To further assess the resulting impact on heat dissipation, transient thermoreflectance was utilized to precisely quantify the thermal transport within the heterostructures. Classical molecular dynamics (MD) simulations were then performed to analyze the underlying physical mechanisms, revealing that intensifying C diffusion increases the phonon density of states overlap and effectively reduces the TBR. Furthermore, the intrinsic stress was quantified through geometric phase analysis (GPA) based on TEM images, demonstrating that the stress induced during the diffusion process propagates to the AlGaN/GaN heterostructure. Crucially, this stress modulation enhances the piezoelectric polarization by approximately 32%, resulting in a 5% increase in the two-dimensional electron gas (2DEG) sheet density. These findings provide a comprehensive strategy for optimizing the thermal management and mechanical reliability of high-power GaN devices.

Keywords: polycrystalline diamond; carbon diffusion; thermal boundary resistance; stress modulation; AlGaN/GaN heterostructures

Check for updates

Academic Editor: Seiichi Miyazaki

Received: 13 January 2026
Revised: 7 February 2026
Accepted: 9 February 2026
Published: 12 February 2026

Copyright: © 2026 by the authors. Licensee MDPI, Basel, Switzerland. This article is an open access article distributed under the terms and conditions of the Creative Commons Attribution (CC BY) license.

1. Introduction

GaN-based high electron mobility transistors (HEMTs) have emerged as the backbone of next-generation high-power radio frequency (RF) and microwave applications due to their high breakdown voltage and superior electron saturation velocity [1–5]. However, their performance potential is severely restricted by the self-heating effect. As power density increases, heat accumulation within the active region leads to a sharp decline in two-dimensional electron gas (2DEG) mobility, causing a marked degradation in both device characteristics and reliability [6–8]. Therefore, efficient near-junction thermal management has become a critical challenge to fully realize the potential of GaN technology.

To address this, integrating a high thermal conductivity (TC) diamond film on the top of GaN devices is considered the most effective strategy [9–13]. A SiNx dielectric

layer is typically employed to protect the GaN surface from H_2 etching damage before diamond growth. Although the introduction of this amorphous layer solves the integration problem of the diamond/GaN heterostructure, its poor TC and interfacial phonon matching inevitably result in a higher thermal boundary resistance (TBR) at the diamond/GaN interface, which becomes a significant obstacle to the effective upward heat dissipation of GaN devices [14–18]. To overcome this limitation, previous studies have indicated that the specific growth conditions of diamond, particularly the high-power density and chamber pressure, promote the diffusion of C atoms into the SiNx interlayer. This diffusion process facilitates the formation of localized SiC nanocrystals within the amorphous layer. The resulting structural transformation effectively bridges the phonon mismatch and enhances the TC of the dielectric layer, achieving an extremely low TBR [19–22]. To deeply comprehend the internal mechanisms driving these properties, current research increasingly adopts a synergy of experiment and simulation. Specifically, calculations based on Density Functional Theory (DFT) have been employed to elucidate the energetics of carbon (C) diffusion and its interactions with defects or dangling bonds, thereby providing theoretical guidance for understanding the subsequent thermal/electronic transport [23]. Moreover, molecular dynamics (MD) simulations serve as a bridge to macroscopic properties, utilizing interatomic potentials to model the phonon density of states (PDOS) at the mixed interface, thereby capturing the dynamic impact of C-induced crystallization [24]. Despite extensive experimental validation confirming the structural evolution caused by C diffusion, a comprehensive understanding of the governing internal mechanisms and their influence on coupled electro-thermal properties is still lacking. On the one hand, the specific influence of C-induced stress evolution on the TBR necessitates in-depth theoretical study [25,26]. On the other hand, the propagation of stress into the AlGaN/GaN heterojunction and its subsequent modulation of electrical properties through the piezoelectric effect are not yet fully understood [27–29]. Consequently, a combined strategy of experiment and simulation is indispensable to systematically elucidate the impact of C diffusion on the coupled electro-thermal performance of AlGaN/GaN heterostructures.

In this work, we systematically investigated the stress variation induced by varying degrees of C diffusion and its dual impact on the TBR and the electrical characteristics of the AlGaN/GaN heterojunction. MD simulations were employed to verify the influence of C diffusion-induced stress on the TBR. Furthermore, geometric phase analysis (GPA) based on transmission electron microscopy (TEM) was utilized to quantitatively characterize the stress propagation into the AlGaN/GaN heterostructure.

2. Materials and Methods

To elucidate the impact of C diffusion induced stress on the coupled electro-thermal performance, samples with identical epitaxial structures were prepared on SiC substrates. The heterostructure consisted of a 1.4 μm GaN buffer, a 0.8 nm AlN interlayer, and a 25 nm $Al_{0.25}Ga_{0.75}N$ barrier. A ~40 nm SiNx passivation layer was deposited through metalorganic chemical vapor deposition (MOCVD). During diamond growth, a double-stage process was employed to balance the competing effects of etching and deposition by adjusting the growth parameters. In the nucleation stage, the extent of C diffusion was controlled by tuning the plasma power density, chamber pressure, and growth temperature, thereby enabling the fabrication of samples with varying dielectric layer thicknesses and C diffusion levels.

To measure the thermal properties of the diamond/SiNx/GaN interfaces, the transient thermoreflectance (TTR) method was utilized [30–32]. The TTR system uses a 355 nm pulse laser as the pump beam. Pulse laser irradiates the sample and produces heating in the surface, which penetrates into the interior of the sample and passes through each material.

A continuous wave (CW) 532 nm laser was used as the probe beam, focused on the sample, and co-axial aligned with the pump beam. Au/Ti metal transducers (80 nm/5 nm) are deposited on the surface of the diamond. The metal transducers generate quantifiable thermal signals from the surface by having a precise linear relationship between reflectance change ($\Delta R/R$) and temperature change (ΔT). The temperature change signal carried by the reflected probe beam is detected by a photodetector (with a bandwidth of 400 MHz) and displayed on a digital oscilloscope (with a bandwidth of 500 MHz).

To complement the experimental investigation and provide atomistic insights into the role of C diffusion, molecular dynamics (MD) simulations were conducted using LAMMPS (Large-scale Atomic/Molecular Massively Parallel Simulator) to investigate the diffusion behavior of C atoms within amorphous SiNx layers. The amorphous SiNx layer was generated using a melt-quench protocol [33–35]. The simulation domain employed periodic boundary conditions along the x- and y-directions, while fixed boundary conditions were maintained in the z-direction to ensure proper heat flow analysis. The Lennard–Jones (LJ) potential was implemented to characterize the atomic pair interactions between localized SiC crystalline and amorphous SiNx. The specific potential function for the SiC is described in the references [36]. To evaluate vibrational matching at the interface, the *PDOS* was calculated for various configurations [37,38]. The AlGaN layer in contact with the interlayer is described using the Stillinger–Weber (SW) potential, with dimensions commensurate with the actual film size [39].

3. Results and Discussion

The microstructural characteristics of the fabricated heterostructures were examined using TEM, as shown in Figure 1. Both samples A and B exhibited a continuous AlGaN/GaN heterostructure capped with an approximately 40 nm SiNx dielectric layer, which effectively protects the GaN surface from H_2 etching during diamond growth. Despite the identical initial SiNx thickness, varying plasma power densities, chamber pressures, and growth temperatures during diamond synthesis resulted in different degrees of C diffusion. The scanning transmission electron microscopy (STEM) image in Figure 1c,d further confirms the layer thicknesses and reveals that the C diffusion exhibits an island-like distribution, consistent with the island nucleation mechanism of diamond growth. In sample A, a 15 nm thick C diffusion layer was observed together with a remaining 25 nm amorphous SiNx layer. In contrast, sample B showed a reduced C incorporation with a 10 nm diffusion layer and a 30 nm SiNx layer [40]. These observations establish a clear correlation between the extent of C diffusion and the remaining SiNx thickness, providing a structural foundation for subsequent TBR analysis and polarization effect investigations.

To further verify the nature of the diffusion layer observed in the TEM images, energy-dispersive X-ray spectroscopy (EDS) mapping was performed for C, silicon (Si), gallium (Ga), and nitrogen (N) elements, as shown in Figure 2. The elemental distributions clearly reveal that both samples exhibited C diffusion into the SiNx dielectric layer, leading to the formation of a SiC layer, while no penetration into the GaN region was detected [19,22]. In sample A, the extent of C diffusion was more pronounced, resulting in a thicker SiC layer and a correspondingly thinner amorphous SiNx layer. In contrast, sample B showed a similar transformation but with reduced C incorporation, leading to a relatively thicker SiNx layer. The thicknesses of the diffusion and dielectric layers determined from EDS mapping were consistent with those obtained from TEM observations, thereby confirming that the contrast variations observed in the TEM images originated from C diffusion.

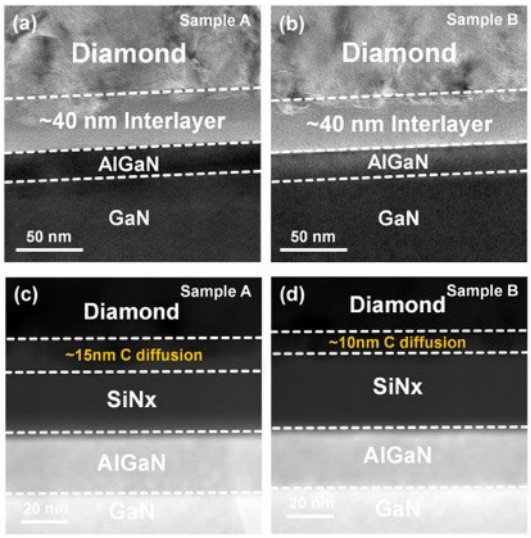


Figure 1. Cross-sectional TEM microstructure of the diamond/GaN interfaces of (**a**) sample A and (**b**) sample B; corresponding STEM images showing interfacial regions of (**c**) samples A and (**d**) sample B.

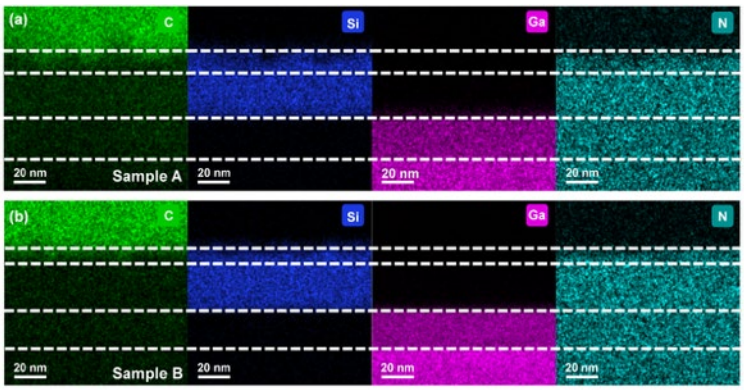


Figure 2. Elemental EDS mapping of (**a**) sample A and (**b**) sample B, showing the distributions of C, Si, Ga, and N.

3.1. Impact of Stress on Heterojunction Thermal Transport

To evaluate the thermal properties of the diamond/SiNx/GaN interfaces, the TTR results are presented in Figure 3. The measured TTR signal is fitted using an analytical heat conduction model (by Global Optimization in MATLAB R2021a) to extract the unknown thermophysical properties of the measured samples [41]. As illustrated in Figure 3a, the Ti layer is incorporated into the effective TBR of the Au/diamond interface ($TBR_{eff,\ Au/Dia}$). Similarly, the AlGaN barrier and GaN buffer are treated as a single GaN layer, while the diamond/SiNx, SiNx, and SiNx/GaN interfaces are collectively represented as the effective TBR of the diamond/GaN interface ($TBR_{eff,\ Dia/GaN}$). Figure 3b shows the measured TTR transients for representative samples A and B, with the best fitting curves overlaid with the measured transients, where the TTR transients of samples A and B highlight clear differences in heat dissipation behavior. Furthermore, Figure 3c presents the comparative fitting results and error analysis for samples A and B. Sample A, characterized by a thicker C diffusion layer and thinner amorphous SiNx dielectric, exhibited a lower TBR compared to sample B. In contrast, the reduced C incorporation and relatively thicker SiNx layer in sample B resulted in a higher TBR.

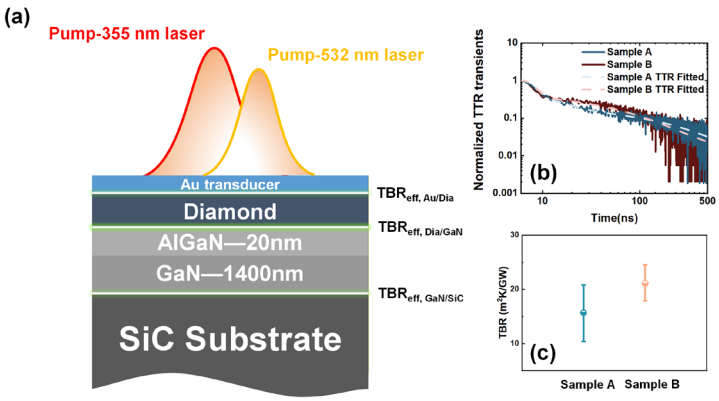


Figure 3. (**a**) Schematic of diamond/SiNx/GaN multilayer composite structure used for TTR measurements. (**b**) TTR transients measured on sample A and sample B with best fitting curves overlaid with the measured transients. (**c**) Comparative fitting results and TBR error analysis for Samples A and B.

Further structural analysis revealed that increased C diffusion promoted partial crystallization within the amorphous SiNx layer while simultaneously reducing its residual thickness, both of which contributed to a lower TBR. To investigate this mechanism, MD simulations were conducted using LAMMPS with the modeling framework illustrated in Figure 4a. The model domain consisted of a top SiC layer, a middle diffusion layer combining amorphous SiNx and SiC, and a bottom amorphous SiNx layer. As shown in Figure 4b–d, with increasing C diffusion, the PDOS of the interlayer gradually shifted toward that of SiC, leading to a significantly larger overlap with AlGaN vibrations. This enhanced phonon coupling provides a microscopic explanation for the experimentally observed reduction in thermal boundary resistance. Previous studies have demonstrated that increased C diffusion enhances the thermal conductivity of the diffusion layer, thereby reducing the overall TBR. Furthermore, the simulation indicates that the crystallization of SiC alters the internal layer structure, enlarging the overlap of the PDOS between the diffusion layer and the AlGaN region, which in turn lowers the interfacial resistance at the lower interface. The underlying reason may be attributed to the modification of phonon velocity with increasing C diffusion. According to the DMM, such variation in phonon velocity enhances the transmission coefficient between the two materials, reduces phonon scattering probability, and consequently decreases the interfacial thermal resistance [42,43].

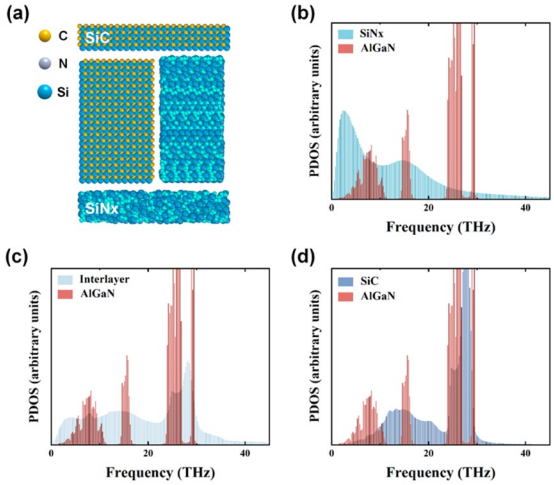


Figure 4. (**a**) Schematic of the MD model structure. PDOS comparison of the (**b**) SiNx layer, (**c**) interlayer, and (**d**) SiC layer with AlGaN in the diamond/GaN heterostructures.

3.2. Impact of Stress on AlGaN/GaN Polarization Effects

In addition to its influence on interfacial thermal transport, the stress induced by C diffusion significantly affects the polarization effects of the AlGaN/GaN heterostructure. During the high-temperature growth of diamond, C diffuses into amorphous SiNx and causes local crystallization, which changes the internal structure and creates stress. As the C diffusion becomes more intense and the SiNx layer becomes thinner, the impact of stress on the interface becomes more significant, which eventually causes stronger lattice strain in the AlGaN layer. The piezoelectric polarization, which originates from lattice mismatch and strain at the heterointerface, directly governs the formation and density of the 2DEG. As the lattice of AlGaN changes, the polarization within the heterojunction is also modified [44].

To quantitatively evaluate this stress distribution, geometric phase analysis (GPA) was performed on high-resolution TEM images, as shown in Figure 5. Both samples exhibited comparable AlGaN/GaN layer thicknesses, providing a consistent basis for strain comparison. The corresponding fast Fourier transform (FFT) patterns of the heterointerfaces are presented in Figure 5(a_1,b_1), where the strongest conjugate diffraction spots in the horizontal and vertical directions were selected. These reflections were used to reconstruct the stress field distributions along both orientations, with the unstrained GaN buffer serving as the zero-strain reference. During the calculation, strain profiles were integrated perpendicular to the interface, and average strain values were extracted from the bulk region of the AlGaN barrier to eliminate interfacial peaks [28,29].

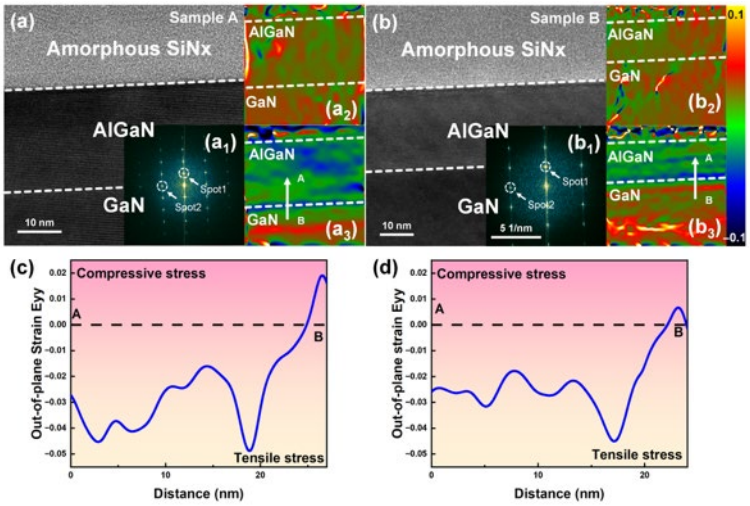


Figure 5. TEM images of AlGaN/GaN heterostructures for (**a**) sample A and (**b**) sample B. Selected FFT patterns used for GPA analysis of ($\mathbf{a_1}$) sample A and ($\mathbf{b_1}$) sample B, and the corresponding strain maps along the xx and yy directions of ($\mathbf{a_2}$,$\mathbf{a_3}$) sample A and ($\mathbf{b_2}$,$\mathbf{b_3}$) sample B. Line-scan profiles extracted from the strain maps of (**c**) sample A and (**d**) sample B.

The in-plane (ε_{xx}) and out-of-plane strain (ε_{yy}) distribution maps for both samples are displayed in Figure 5(a_2,a_3,b_2,b_3). For the ε_{xx} maps, no distinct boundary or discontinuity was observed across the heterointerface. In contrast, the ε_{yy} maps exhibited a sharp discontinuity due to lattice mismatch and Poisson effect [45]. A localized strain peak was consistently observed at the immediate interface, reflecting atomic-scale distortion. As shown in Figure 5c,d, line-scan profiles along the A–B direction further confirmed that sample A, with stronger C diffusion and a thinner SiNx dielectric, introduced enhanced tensile stress into the AlGaN region. In contrast, sample B showed weaker stress modulation. By averaging the bulk strain values, the compressive strain was determined to increase from –0.025 in sample B to –0.033 in sample A, corresponding to a 32% enhancement in

stress within the AlGaN barrier. According to piezoelectric theory, this mechanical gain leads to a proportional increase in the piezoelectric polarization component. Considering the dilution effect of spontaneous polarization in GaN-based heterostructures, the 32% stress enhancement is theoretically translated into a net increase of approximately 5% in the 2DEG sheet density [46,47].

4. Conclusions

In conclusion, C diffusion-induced stress modulation exerts a dual positive effect on AlGaN/GaN heterostructures. By controlling the C diffusion depth to approximately 15 nm within the 40 nm SiNx interlayer, the TBR is reduced due to better phonon transmission. At the same time, this C-induced stress effectively changes the lattice strain in the AlGaN layer, leading to a 32% increase in piezoelectric polarization and a 5% enhancement in the 2DEG sheet density. These quantitative results suggest that increasing the C diffusion intensity while keeping the AlGaN/GaN interface intact is a practical way to improve both the thermal and electrical performance of GaN devices.

Author Contributions: Conceptualization, H.S. and M.W.; methodology, M.W. and L.Y.; software, M.W. and C.Y.; validation, H.S. and P.X.; formal analysis, H.S. and P.X.; investigation, H.S., H.L., B.H. and M.Z.; resources, M.W., C.Y., L.Y., X.M. and Y.H.; data curation, H.S. and P.X.; writing—original draft preparation, H.S.; writing—review and editing, H.S. and M.W.; visualization, H.S. and P.X.; supervision, X.M. and Y.H.; project administration, M.W., C.Y., X.M. and Y.H.; funding acquisition, M.W. and L.Y. All authors have read and agreed to the published version of the manuscript.

Funding: This research was supported in part by the National Natural Science Foundation of China under grants 62574152, 62234009 and 62188102 and in part by the China Postdoctoral Science Foundation under grant 2022T150505.

Data Availability Statement: The datasets presented in this article are not readily available because the data are part of an ongoing study. Requests to access the datasets should be directed to corresponding author.

Conflicts of Interest: The authors declare no conflicts of interest.

References

1. Millan, J.; Godignon, P.; Perpina, X.; Perez-Tomas, A.; Rebollo, J. A Survey of Wide Bandgap Power Semiconductor Devices. *IEEE Trans. Power Electron.* **2014**, *29*, 2155–2163. [CrossRef]
2. Okumura, H. Present Status and Future Prospect of Widegap Semiconductor High-Power Devices. *Jpn. J. Appl. Phys.* **2006**, *45*, 7565–7586. [CrossRef]
3. Mishra, U.K.; Parikh, P.; Wu, Y.-F. AlGaN/GaN HEMTs-An Overview of Device Operation and Applications. *Proc. IEEE* **2002**, *90*, 1022–1031. [CrossRef]
4. Mishra, U.K.; Shen, L.; Kazior, T.E.; Wu, Y.F. GaN-Based RF Power Devices and Amplifiers. *Proc. IEEE* **2008**, *96*, 287–305. [CrossRef]
5. Kikkawa, T.; Makiyama, K.; Ohki, T.; Kanamura, M.; Imanishi, K.; Hara, N.; Joshin, K. High Performance and High Reliability AlGaN/GaN HEMTs. *Phys. Status Solidi (A) Appl. Mater. Sci.* **2009**, *206*, 1135–1144. [CrossRef]
6. Gaska, R.; Osinsky, A.; Yang, J.W.; Shur, M.S. Self-Heating in High-Power AlGaN-GaN HFET's. *IEEE Electron Device Lett.* **1998**, *19*, 89–91. [CrossRef]
7. Wu, M.; Ma, X.H.; Yang, L.; Zhu, Q.; Zhang, M.; Yang, L.A.; Hao, Y. Accurate Measurement of Channel Temperature for AlGaN/GaN HEMTs. *IEEE Trans. Electron Devices* **2018**, *65*, 4792–4799. [CrossRef]
8. Filippov, K.A.; Balandin, A.A. The Effect of the Thermal Boundary Resistance on Self-Heating of AlGaN/GaN HFETs. *MRS Internet J. Nitride Semicond. Res.* **2003**, *8*, e4. [CrossRef]
9. Gurbuz, Y.; Esame, O.; Tekin, I.; Kang, W.P.; Davidson, J.L. Diamond Semiconductor Technology for RF Device Applications. *Solid State Electron.* **2005**, *49*, 1055–1070. [CrossRef]
10. Tadjer, M.J.; Anderson, T.J.; Hobart, K.D.; Feygelson, T.I.; Caldwell, J.D.; Eddy, C.R.; Kub, F.J.; Butler, J.E.; Pate, B.; Melngailis, J. Reduced Self-Heating in AlGaN/GaN HEMTs Using Nanocrystalline Diamond Heat-Spreading Films. *IEEE Electron Device Lett.* **2012**, *33*, 23–25. [CrossRef]

11. Meyer, D.J.; Koehler, A.D.; Hobart, K.D.; Eddy, C.R.; Feygelson, T.I.; Anderson, T.J.; Roussos, J.A.; Tadjer, M.J.; Downey, B.P.; Katzer, D.S.; et al. Large-Signal RF Performance of Nanocrystalline Diamond Coated AlGaN/GaN High Electron Mobility Transistors. *IEEE Electron Device Lett.* **2014**, *35*, 1013–1015. [CrossRef]
12. Wu, M.; Cheng, K.; Yang, L.; Hou, B.; Zhang, X.C.; Wang, P.; Zhang, M.; Zhu, Q.; Zheng, X.F.; Hu, Y.S.; et al. Structural and Thermal Analysis of Polycrystalline Diamond Thin Film Grown on GaN-on-SiC with an Interlayer of 20 Nm PECVD-SiN. *Appl. Phys. Lett.* **2022**, *120*, 121603. [CrossRef]
13. Soman, R.; Malakoutian, M.; Shankar, B.; Field, D.; Akso, E.; Hatui, N.; Hines, N.J.; Graham, S.; Mishra, U.K.; Kuball, M.; et al. Novel All-around Diamond Integration with GaN HEMTs Demonstrating Highly Efficient Device Cooling. In *Proceedings of the 2022 International Electron Devices Meeting (IEDM), San Francisco, CA, USA, 3 December 2022*; IEEE: New York, NY, USA, 2022; pp. 30.8.1–30.8.4.
14. Sun, H.; Simon, R.B.; Pomeroy, J.W.; Francis, D.; Faili, F.; Twitchen, D.J.; Kuball, M. Reducing GaN-on-Diamond Interfacial Thermal Resistance for High Power Transistor Applications. *Appl. Phys. Lett.* **2015**, *106*, 111906. [CrossRef]
15. Cho, J.; Francis, D.; Altman, D.H.; Asheghi, M.; Goodson, K.E. Phonon Conduction in GaN-Diamond Composite Substrates. *J. Appl. Phys.* **2017**, *121*, 055105. [CrossRef]
16. Zhou, Y.; Anaya, J.; Pomeroy, J.; Sun, H.; Gu, X.; Xie, A.; Beam, E.; Becker, M.; Grotjohn, T.A.; Lee, C.; et al. Barrier-Layer Optimization for Enhanced GaN-on-Diamond Device Cooling. *ACS Appl. Mater. Interfaces* **2017**, *9*, 34416–34422. [CrossRef]
17. Yates, L.; Anderson, J.; Gu, X.; Lee, C.; Bai, T.; Mecklenburg, M.; Aoki, T.; Goorsky, M.S.; Kuball, M.; Piner, E.L.; et al. Low Thermal Boundary Resistance Interfaces for GaN-on-Diamond Devices. *ACS Appl. Mater. Interfaces* **2018**, *10*, 24302–24309. [CrossRef]
18. Zhou, H.; Feng, T. Theoretical Upper Limits of the Thermal Conductivity of Si_3N_4. *Appl. Phys. Lett.* **2023**, *122*, 182203. [CrossRef]
19. Malakoutian, M.; Field, D.E.; Hines, N.J.; Pasayat, S.; Graham, S.; Kuball, M.; Chowdhury, S. Record-Low Thermal Boundary Resistance between Diamond and GaN-on-SiC for Enabling Radiofrequency Device Cooling. *ACS Appl. Mater. Interfaces* **2021**, *13*, 60553–60560. [CrossRef]
20. Woo, K.; Malakoutian, M.; Jo, Y.; Zheng, X.; Pfeifer, T.; Mandia, R.; Hwang, T.; Aller, H.; Field, D.; Kasperovich, A.; et al. Interlayer Engineering to Achieve <1 m^2 K/GW Thermal Boundary Resistances to Diamond for Effective Device Cooling. In *Proceedings of the Institute of Electrical and Electronics Engineers (IEEE), San Francisco, CA, USA, 7 February 2024*; IEEE: New York, NY, USA, 2024; pp. 1–4.
21. Sun, H.; Wu, M.; Wang, P.; Yuan, C.; Ma, G.; Yang, L.; Ma, X.; Hao, Y. Comparison of SiNx Dielectric Layer Grown by Plasma-Enhanced Chemical Vapor Deposition, Low-Pressure Chemical Vapor Deposition, and Metal-Organic Chemical Vapor Deposition in Diamond- and GaN-Based Integrated Devices. *Phys. Status Solidi B Basic Res.* **2024**, *261*, 2400052. [CrossRef]
22. Wang, Y.; Zhou, B.; Ma, G.; Zhi, J.; Yuan, C.; Sun, H.; Ma, Y.; Gao, J.; Wang, Y.; Yu, S. Effect of Bias-Enhanced Nucleation on the Microstructure and Thermal Boundary Resistance of GaN/SiNx/Diamond Multilayer Composites. *Mater. Charact.* **2023**, *201*, 112985. [CrossRef]
23. Furlan, A.; Gueorguiev, G.K.; Högberg, H.; Stafström, S.; Hultman, L. Fullerene-like CPx: A First-Principles Study of the Relative Stability of Precursors and Defect Energetics during Synthetic Growth. *Thin Solid Films* **2006**, *515*, 1028–1032. [CrossRef]
24. Xu, B.; Mu, F.; Liu, Y.; Guo, R.; Hu, S.; Shiomi, J. Record-Low Thermal Boundary Resistance at Bonded GaN/Diamond Interface by Controlling Ultrathin Heterogeneous Amorphous Layer. *Acta Mater.* **2025**, *282*, 120458. [CrossRef]
25. Swartz, E.T.; Pohl, R.O. Thermal Boundary Resistance. *Rev. Mod. Phys.* **1989**, *61*, 605. [CrossRef]
26. De Bellis, L.; Phelan, P.E.; Prasher, R.S. Variations of Acoustic and Diffuse Mismatch Models in Predicting Thermal-Boundary Resistance. *J. Thermophys. Heat Trans.* **2000**, *14*, 144–150. [CrossRef]
27. Ambacher, O.; Foutz, B.; Smart, J.; Shealy, J.R.; Weimann, N.G.; Chu, K.; Murphy, M.; Sierakowski, A.J.; Schaff, W.J.; Eastman, L.F.; et al. Two Dimensional Electron Gases Induced by Spontaneous and Piezoelectric Polarization in Undoped and Doped AlGaN/GaN Heterostructures. *J. Appl. Phys.* **2000**, *87*, 334–344. [CrossRef]
28. Anwar, A.F.M.; Webster, R.T.; Smith, K.V. Bias Induced Strain in AlGaN/GaN Heterojunction Field Effect Transistors and Its Implications. *Appl. Phys. Lett.* **2006**, *88*, 203510. [CrossRef]
29. Smorchkova, I.P.; Elsass, C.R.; Ibbetson, J.P.; Vetury, R.; Heying, B.; Fini, P.; Haus, E.; DenBaars, S.P.; Speck, J.S.; Mishra, U.K. Polarization-Induced Charge and Electron Mobility in AlGaN/GaN Heterostructures Grown by Plasma-Assisted Molecular-Beam Epitaxy. *J. Appl. Phys.* **1999**, *86*, 4520–4526. [CrossRef]
30. Yuan, C.; Hanus, R.; Graham, S. A Review of Thermoreflectance Techniques for Characterizing Wide Bandgap Semiconductors' Thermal Properties and Devices' Temperatures. *J. Appl. Phys.* **2022**, *132*, 220701. [CrossRef]
31. Yuan, C.; Meng, B.; Mao, Y.; Wu, M.; Jia, F.; Yang, L.; Ma, X.; Hao, Y. Transducer-Less Thermoreflectance Technique for Measuring Thermal Properties of the Buried Buffer Layer and Interface in GaN-Based HEMTs. *ACS Appl. Electron. Mater.* **2022**, *4*, 5984–5995. [CrossRef]
32. Yuan, C.; Pomeroy, J.W.; Kuball, M. Above Bandgap Thermoreflectance for Non-Invasive Thermal Characterization of GaN-Based Wafers. *Appl. Phys. Lett.* **2018**, *113*, 102101. [CrossRef]
33. Lambrecht, A.; Ori, G.; Massobrio, C.; Boero, M.; Martin, E. Assessing the Thermal Conductivity of Amorphous SiN by Approach-to-Equilibrium Molecular Dynamics. *J. Chem. Phys.* **2024**, *160*, 094505. [CrossRef]

34. Larkin, J.M.; McGaughey, A.J.H. Thermal Conductivity Accumulation in Amorphous Silica and Amorphous Silicon. *Phys. Rev. B Condens. Matter Mater. Phys.* **2014**, *89*, 144303. [CrossRef]
35. Liao, Y.; Shiomi, J. Akhiezer Mechanism Dominates Relaxation of Propagons in Amorphous Material at Room Temperature. *J. Appl. Phys.* **2021**, *130*, 035101. [CrossRef]
36. Tersoff, J. Modeling Solid-State Chemistry: Interatomic Potentials for Multicomponent Systems. *Phys. Rev. B* **1989**, *39*, 5566–5568. [CrossRef] [PubMed]
37. Hu, M.; Zhang, X.; Poulikakos, D.; Grigoropoulos, C.P. Large "near Junction" Thermal Resistance Reduction in Electronics by Interface Nanoengineering. *Int. J. Heat Mass Transf.* **2011**, *54*, 5183–5191. [CrossRef]
38. Gu, L.; Li, Y.; Shen, Y.; Yang, R.Y.; Ma, H.P.; Sun, F.; Zuo, Y.; Tang, Z.; Yuan, Q.; Jiang, N.; et al. A Strategy for Enhancing Interfacial Thermal Transport in Ga_2O_3-Diamond Composite Structure by Introducing an AlN Interlayer. *Nano Energy* **2024**, *132*, 110389. [CrossRef]
39. Zhang, L.; Yan, H.; Zhu, G.; Liu, S.; Gan, Z.; Zhang, Z. Effect of Substrate Surface on Deposition of AlGaN: A Molecular Dynamics Simulation. *Crystals* **2018**, *8*, 279. [CrossRef]
40. Malakoutian, M.; Ren, C.; Woo, K.; Li, H.; Chowdhury, S. Development of Polycrystalline Diamond Compatible with the Latest N-Polar GaN Mm-Wave Technology. *Cryst. Growth Des.* **2021**, *21*, 2624–2632. [CrossRef]
41. Ma, G.; Wang, Y.; Xia, R.; Meng, B.; Yuan, S.; Zhou, B.; Yuan, C. Modulating Microstructure and Thermal Properties of Diamond/SiNx/GaN Multilayer Structure by Diamond Growth Temperature. *Diam. Relat. Mater.* **2024**, *141*, 110717. [CrossRef]
42. Luo, H.; Zhu, L. Effects of Surface Stress on the Phonon Properties in GaN Nanofilms. *J. Appl. Mech.* **2015**, *82*, 111002. [CrossRef]
43. Ji, X.; Vanjari, S.C.; Francis, D.; Cuenca, J.A.; Nandi, A.; Cherns, D.; Williams, O.A.; Ejeckam, F.; Pomeroy, J.W.; Kuball, M. Thermal Boundary Resistance Reduction by Interfacial Nanopatterning for GaN-on-Diamond Electronics Applications. *ACS Appl. Electron. Mater.* **2025**, *7*, 2939–2946. [CrossRef]
44. Deng, C.; Wang, P.; Tang, C.; Hu, Q.; Du, F.; Jiang, Y.; Zhang, Y.; Li, M.; Xiong, Z.; Wang, X.; et al. Improvement of DC Performance and RF Characteristics in GaN-Based HEMTs Using SiNx Stress-Engineering Technique. *Nanomaterials* **2024**, *14*, 1471. [CrossRef]
45. Lurie, A.I.; Belyaev, A. *Theory of Elasticity*; Springer: Berlin/Heidelberg, Germany, 2005; ISBN 978-3-540-24556-8.
46. Bernardini, F.; Fiorentini, V.; Vanderbilt, D. Spontaneous Polarization and Piezoelectric Constants of III-V Nitrides. *Phys. Rev. B* **1997**, *56*, R10024–R10027. [CrossRef]
47. Ambacher, O.; Smart, J.; Shealy, J.R.; Weimann, N.G.; Chu, K.; Murphy, M.; Schaff, W.J.; Eastman, L.F.; Dimitrov, R.; Wittmer, L.; et al. Two-Dimensional Electron Gases Induced by Spontaneous and Piezoelectric Polarization Charges in N- and Ga-Face AlGaN/GaN Heterostructures. *J. Appl. Phys.* **1999**, *85*, 3222–3233. [CrossRef]

Disclaimer/Publisher's Note: The statements, opinions and data contained in all publications are solely those of the individual author(s) and contributor(s) and not of MDPI and/or the editor(s). MDPI and/or the editor(s) disclaim responsibility for any injury to people or property resulting from any ideas, methods, instructions or products referred to in the content.